Journal of Magnetism and Magnetic Materials 326 (2013) 14–21

Contents lists available at SciVerse ScienceDirect

Journal of Magnetism and Magnetic Materials

journal homepage: www.elsevier.com/locate/jmmm

Simple models for the heating curve in magnetic hyperthermia experiments

G.T. Landi *

Instituto de Física da Universidade de São Paulo, 05314-970 São Paulo, Brazil

ARTICLE INFO

Article history:
Received 27 April 2012
Received in revised form
24 July 2012
Available online 31 August 2012

Keywords:
Magnetic hyperthermia
Single-domain particles
Dynamic hysteresis

ABSTRACT

The use of magnetic nanoparticles for magnetic hyperthermia cancer treatment is a rapidly developing field of multidisciplinary research. From the material's standpoint, the main challenge is to optimize the heating properties of the material while maintaining the frequency of the exciting field as low as possible to avoid biological side effects. The figure of merit in this context is the specific absorption rate (SAR), which is usually measured from calorimetric experiments. Such measurements, which we refer to as heating curves, contain a substantial amount of information regarding the energy barrier distribution of the sample. This follows because the SAR itself is a function of temperature, and reflect the underlying magneto-thermal properties of the system. Unfortunately, however, this aspect of the problem is seldom explored and, commonly, only the SAR at ambient temperature is extracted from the heating curve. In this paper we introduce a simple model capable of describing the entire heating curve via a single differential equation. The SAR enters as a forcing term, thus facilitating the use of different models for it. We discuss in detail the heating in the context of Néel relaxation and show that high anisotropy samples may present an inflection point related to the reduction of the energy barrier caused by the increase in temperature. Mono-disperse and poli-disperse systems are discussed in detail and a new alternative to compute the temperature dependence of the SAR from the heating curve is presented.

1. Introduction

The basic idea behind magnetic hyperthermia is to explore the energy dissipated as heat when magnetic nanoparticles are excited by an external high frequency magnetic field [1–8]. On the one hand this process is of substantial academic interest in light of the intricate relation between the heating power and the magnetic properties of the material [9–14]. On the other hand, several applications based on this technique have also been proposed [15,16], the most notable of which is in oncology, where the nanoparticles are used as local heating centers to eliminate tumorous cells [8,17,18].

Magnetic hyperthermia experiments usually measure the temperature variation of the sample under the application of a time varying magnetic field, commonly approximated by a harmonic wave of the form $H(t) = H_0 \cos \omega t$. The specific absorption rate (SAR) — a figure of merit of the experiment — is usually the only extracted parameter, computed from the initial slope of the measured data. Such procedure clearly squanders valuable information. For, embedded in the heating curve are details concerning the entire temperature dependence of the SAR. To illustrate the importance of such knowledge, note that in practically all dynamical models describing the magnetic properties of nanoparticles [11], the temperature (T) always appears in ratios of the form E/kT, where E is some effective barrier which, more often than not, is the fundamental quantity dictating the magnetic properties of the system. Whence, from knowledge of the temperature dependence of the SAR, one may extract information (qualitative at least) about the distribution of energy barriers in the system.

Several authors have also reported the existence of heating curves with an inflection point at small times (being initially convex instead of concave) [2,7,19,20]. One may argue that these initial points reflect an intrinsic response time of the experimental setup and should thence be discarded (e.g., transients in the coil which produce the magnetic field). Even though this is in fact true, it has also been reported that the response time may actually vary from one sample to another, an effect whose physical interpretation is not immediately obvious. Indeed, as we show in this paper, samples with high magnetic anisotropy may present an inflection point that is entirely unrelated to any response times. As we discuss, this is a direct consequence of the fact that the SAR is itself a function of temperature which, for some systems, may vary significantly over the temperature ranges involved in the experiment. Clearly, such property may incite altercations as to what value best represents the SAR and,

* Tel.: +55 113 091 7081.
E-mail address: gtlandi@gmail.com

0304-8853/$ - see front matter © 2012 Elsevier B.V. All rights reserved.
http://dx.doi.org/10.1016/j.jmmm.2012.08.034

more importantly, what impact this may have on actual oncological treatments.

In this paper we discuss a simple model to describe the heating curve in magnetic hyperthermia experiments. Besides its simplicity, this model also provides a direct link between the calorimetric and magnetic properties of the nanoparticles. Albeit not our primary goal, we also propose a new method of data analysis that, with sufficient care, may be successfully employed to extract information from real systems. More importantly, however, it is our hope that the present discussion may provide additional insight into the physical processes taking place in this important experiment.

The vast range of experimental systems (including *in vivo* experiments) clearly inhibits a general treatment of the problem. Thus, our focus is on a framework that is simple enough to represent at least a broad range of conditions. In this sense, it is interesting to avoid model containing spatial variables, as e.g., temperature gradients. For these would result in partial differential equations that are strongly dependent on the boundary conditions of the experiment. We thus approach the problem from the viewpoint of lumped element models; that is, we replace spatially distributed systems with discrete entities that approximate the real system under certain conditions. This allows us to describe the heating curve via a simple ordinary differential equation (DE), which is not only more easily tractable, but also more general: all properties of a given system are entirely represented by parameters appearing in the DE and may, therefore, be fitted from experiment.

The starting point for our analysis is based on the following very important argument. During the heating experiment the particle ensemble continually undergoes dynamic hysteresis loops with a period of $\sim 10^{-5}$ s. Energy is thus being continually dissipated, with a rate that depends not only on the external field and the magnetic properties of the sample, but also on the temperature, which itself changes during the experiment. In this sense, the system should never reach a *steady state*. However, the time scales of heat conduction are much larger than the average hysteresis cycle (heating experiments extend well beyond hundreds of seconds). Thus, at every instant, the average power dissipated by the nanoparticles in the form of heat (S), may be taken to a very good approximation as an average over a large number of steady state hysteresis cycles; that is, we write $S = S(T)$.

In Section 2 we define the proposed model and discuss some of its basic properties. In order to provide a definite example to illustrate its applicability, we briefly discuss the linear response Néel relaxation in Section 3. Then, in Section 4, the heating curves simulated using Néel relaxation within the developed model are analyzed in detail for mono-disperse systems. The subject of polidispersivity, of fundamental importance in real systems, is discussed in Section 5. In Section 6 we present a method to extract the temperature dependence of the SAR from the experimental data. In Section 7 we briefly discuss a model of two temperatures, whose intent is to describe the difference between the temperature of the particles and that of the fluid. Finally, Section 8 provides an additional discussion and summarizes the most relevant conclusions.

2. Single temperature model

To study the heating curve, the simplest approach is to assume that the temperature is homogenous throughout the sample, being only a function time. This is motivated by the random spatial arrangement of the nanoparticles within it, which entail a somewhat uniform heating. Let us first consider the system in the absence of an external field. Then, according to Le Chatelier's principle, any changes in the equilibrium between the sample and the environment should prompt an opposing reaction to counteract this change. For the present case — where these arguments are also sometimes referred to as Newton's law of cooling — this implies that the rate of heat loss ($\dot{Q}$) is proportional to the difference in temperature between the sample (T) and the medium (T_e), viz.,

$$\dot{Q} = a_1(T_e - T), \tag{1}$$

where a_1 is a constant whose order of magnitude is that of the thermal conductivity of the magnetic fluid times the characteristic length of the sample. If we assume a constant specific heat (C), we may write $\dot{Q} = C\dot{T}$. Then, defining $a = a_1/C$ and changing variables to $\Gamma = T - T_e$ we arrive at

$$\dot{\Gamma} = -a\Gamma, \tag{2}$$

whose solution is $\Gamma(t) = \Gamma(0)\exp(-at)$. Whence, Eq. (1) states that when the system is momentarily disturbed from equilibrium with the thermal bath, its tendency will be to return exponentially to the original state with characteristic time, a^{-1}. We refer to this as the *cooling curve*. It may be computed as an extension of the heating curve, continuing the data acquisition after the external field has been shut off. A graph of $\log(\Gamma)$ vs. t should yield a straight line with slope $-a$, as illustrated by the solid curve in Fig. 1(a). Henceforth, in numerical calculations, we shall usually take $a = 1$ to simplify the discussion, given that its effect is simply to change the time scale. For reference, in real systems $a \sim 10^{-2}\ \mathrm{s}^{-1}$.

It is possible that the cooling curve takes the form shown in dashed lines in Fig. 1(a), represented instead by a sum of decaying exponentials. Quite likely, the main reason for this lies in the heat dissipated by the coil itself. This can be unambiguously verified by heating the sample with an external heat source and measuring the corresponding cooling curve.

The heating curve is obtained from Eq. (2) by introducing the dissipated power as a forcing term

$$\dot{\Gamma} = -a\Gamma + S(\Gamma). \tag{3}$$

The main goal of hyperthermia experiments is to extract $S(\Gamma)$ from $\Gamma(t)$. In our notation, S is given in units of degree per unit time. The SAR, on the other hand, is usually expressed in units of power per unit mass of magnetic material. Whence, it may be computed from S by multiplying by C and dividing by the mass.

At ambient temperature, $\Gamma = 0$, and from the DE (2) we immediately see that

$$S(\Gamma = 0) = \lim_{t\to 0} \dot{\Gamma}(t), \tag{4}$$

which is the usual method of computing the SAR. Within the scope of the current model, this procedure is quite satisfactory

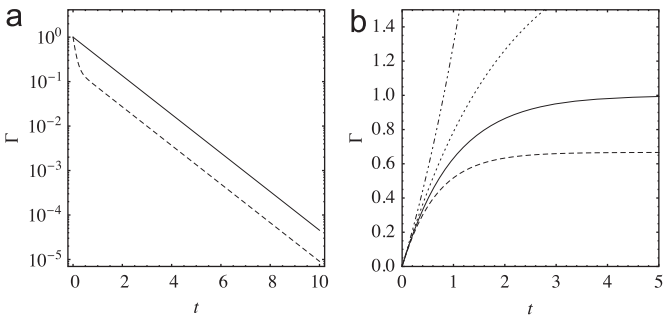

Fig. 1. (a) Example cooling curves. (solid) $\Gamma = e^{-t}$, corresponding to the model in Eq. (2); (dashed) $\Gamma = 0.3e^{-t} + 0.7e^{-5t}$, illustrating the possibility of additional sources of heat (e.g., from the coil). (b) Example heating curves [Eq. (3)] with $a = 1$. (solid) Eq. (5), with $S_0 = 1$. Others are for Eq. (10) with $S_0 = 1$: (dashed) $\alpha = -1/2$, (dotted) $\alpha = 1/2$ and (dot-dashed) $\alpha = 3/2$.

since it has the advantage of being independent of the cooling properties of the sample (viz., a).

If $S(\Gamma)=S_0$ (a constant) then the solution of Eq. (3) is

$$\Gamma(t)=(S_0/a)[1-\exp(-at)]. \tag{5}$$

This function, sometimes referred to as a Box–Lucas, has also been used to fit the data [20] and thence extract S_0 from $\dot{\Gamma}$ in the limit $\Gamma\to 0$. This approach, however, is not adequate. For as we show below, taking $S(\Gamma)$ as a constant may be a quite poor approximation. Thus, since the fit minimizes the merit function for the entire heating curve, it may sacrifice the accuracy at the region where $\Gamma\sim 0$. A typical heating curve for Eq. (5) is illustrated in Fig. 1(b) (solid curve), for $S_0=a=1$. As can be seen, it agrees with the more common result that $\Gamma(t)$ is a concave function (it gives $\ddot{\Gamma}=-aS_0\exp -at$, which is negative for all t).

3. Néel relaxation

We now deviate briefly from the analysis of the heating curve with the purpose of introducing a definite model for $S(\Gamma)$. We consider the situation where H_0 is sufficiently small so that the magnetic response may be taken as linear. This is perhaps the only situation where analytical formulae for $S(\Gamma)$ is readily available. For definiteness, we also consider a system whose dynamics is dictated only by Néel relaxation (precession of the magnetic moment); for instance, a sample in the form of a powder or gel, or one consisting of sufficiently small particles so as to render Néel relaxation dominant over Brownian relaxation (physical rotation of the particle). The latter is in fact our primary motivation for focusing on Néel processes, given the increasing attention that smaller clusters have received in recent years. The reasons for this are mainly biological, concerning colloid stabilization, inter-particle aggregation, embolization, etc.

The usual expression for $S(\Gamma)$ is obtained as follows. Dissipation directly implies hysteresis in a graph of $M(t)$ vs. $H(T)$ [where $M(t)$ is the sample magnetization; this refers to the high frequency dynamic hysteresis loops taking place during the heating curve, not its quasi-static counterpart]. In the linear response regime the magnetization will follow the harmonic field, $H(t)=H_0\cos\omega t$, albeit possibly with a phase lag: $M(t)=H_0(\chi'\cos\omega t-\chi''\sin\omega t)$. Here, χ' and χ'' are respectively the real and imaginary parts of the dynamic susceptibility. Thus the hysteresis loops will always be ellipsis, the area (A) of which is the average energy dissipated per cycle (this follows from the first law of thermodynamics [21]). By direct integration we may write $A=\pi H_0^2\chi''$. The susceptibility, in turn, may be related to the relaxation properties of the system via the Kubo relation [22]. In the event that the relaxation is well described by a single relaxation time τ, this reduces to the famous Debye factor: $\chi''(\omega)=\chi_0\omega\tau/(1+\omega\tau)$, where χ_0 is the static susceptibility. Finally, the dissipated power is simply $S=fA$, where $f=\omega/2\pi$ is the frequency of the magnetic field. Whence

$$S=\frac{\omega H_0^2\chi_0}{2}\frac{\omega\tau}{1+(\omega\tau)^2}. \tag{6}$$

The static susceptibility (χ_0) and the relaxation time (τ) may both be written in terms of $\sigma=Kv/k_BT$, where K is the anisotropy constant and v is the volume of the particle. The susceptibility can be written as [23]

$$\chi_0=\frac{M_s^2}{3K}\frac{1}{2}\left[\frac{\sqrt{\sigma}}{D(\sqrt{\sigma})}-1\right]\simeq\frac{M_s^2}{3K}(\sigma-1),$$

where $D(x)$ is Dawson's integral [24] and M_s is the saturation magnetization. We note that, for $\sigma\gtrsim 2$, the above approximation is, in fact, quite accurate. The relaxation time, on the other hand, is well represented by the Néel–Brown formula [11]

$$\tau=\frac{\tau_0}{2}\sqrt{\frac{\pi}{\sigma}}e^{\sigma}, \tag{7}$$

where $\tau_0\sim 10^{-10}$ s. This expression is also valid for $\sigma\gtrsim 2$ and provides a correction to the main exponential dependence. It is worth pointing that $\sigma<2$ is usually of little interest to hyperthermia, since it gives a negligible dissipation unless high frequencies are employed; this, in turn, is not recommend for it may excite eddy currents inside the patient's body [4]. Finally, it is worth emphasizing the importance of σ, which is the fundamental parameter determining the dynamics of the system in the context of Néel relaxation (cf. the discussion in Section 1).

It is convenient to write Eq. (6) in the form $S(\sigma)=\xi s(\sigma)$, where $\xi=\omega H_0^2M_s^2/6KC$ and

$$s(\sigma)=(\sigma-1)\operatorname{sech}\left(\sigma-\sigma_m+\log\frac{1}{2}\sqrt{\frac{\pi}{\sigma}}\right), \tag{8}$$

with $\sigma_m=-\log\omega\tau_0$. The reason for this choice is as follows. The function $s(\sigma)$ is illustrated in Fig. 2(a) for different values of $\omega\tau_0$. As the hyperbolic secant, it has the form of a sharply peaked distribution; however, it is slightly distorted due to the presence of the terms $\chi_0\propto(\sigma-1)$ and $g(\sigma)$. If both were neglected, the maxima would be precisely at σ_m. Continuing to neglect the influence of χ_0, a further iteration yields the following useful expression for the maxima of $s(\sigma)$:

$$\sigma_{m2}=\sigma_m+1/2\log\sigma_m-\log\sqrt{\pi}/2, \tag{9}$$

accurate to $\sim 5\%$ of the exact value [cf. the dashed lines in Fig. 2(a)]. The importance of σ_{m2} is in the fact that it distinguishes the regions where $S(\Gamma)$ increases or decreases with increasing temperature [illustrated by an arrow in Fig. 2(a)].

To clarify this further, let σ_0 represent the value of σ at ambient temperature, henceforth taken as $T_0=300$ K. To compute the temperature dependence of the SAR we then write $\sigma=\sigma_0/(1+\Gamma/T_0)$. The function $s(\Gamma)$ is illustrated in Fig. 2(b) for different values of σ_0 and $\omega\tau_0=10^{-4}$ [i.e., $\omega/(2\pi)\sim 10^5$ Hz]. In this case, the maxima takes place at $\sigma_{m2}\sim 10.5$. Based on these curves, it is possible to reach the following very important conclusion. For systems with particles in the high barrier regime ($\sigma_0>\sigma_{m2}$) the SAR as a function of temperature will have a positive initial slope [$S'(\Gamma=0)>0$], whereas those in the low barrier regime ($\sigma_0<\sigma_{m2}$) will have a negative initial slope [$S'(\Gamma=0)<0$]. It is important to emphasize that this distinction between low and high barriers is relative to the frequency in question; as seen in Fig. 2(a), such intervals change for different $\omega\tau_0$ (since σ_{m2} changes). Finally, note that Fig. 2(b) also corroborates the assertion made after Eq. (5), that taking $S(\Gamma)$ as a constant is a quite poor approximation. As a final comment, we note that during the heating process some particles eventually

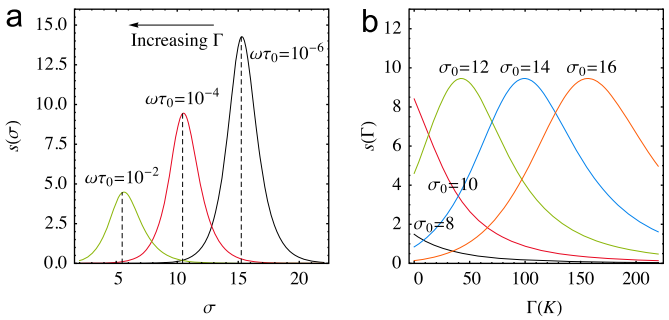

Fig. 2. (a) Reduced SAR, $s(\sigma)$, for different values of $\omega\tau_0$ [Eq. (8)]. The dashed lines were computed using Eq. (9). (b) Similar to image (a), but for the function $s(\Gamma)$ computed using $\sigma=\sigma_0/(1+\Gamma/T_0)$, for different values of σ_0, with fixed $T_0=300$ K and $\omega\tau_0=10^{-4}$.

surpass their Curie temperature. As can be seen in Fig. 2, however, at such stage (high Γ; small σ)their contribution to the overall heating of the sample is already negligible, rendering this effect likely to be unimportant.

4. Analysis of the heating curve for Néel relaxation

Let us now return to the analysis of the DE (3). As a first approximation, we may expand S in powers of Γ up to first order; namely, $S(\Gamma) \simeq S_0 + \alpha\Gamma$. The solution is then precisely the same as that of Eq. (5), but with a replaced by $a-\alpha$

$$\Gamma(t) = \frac{S_0}{a-\alpha}[1-e^{-(a-\alpha)t}]. \tag{10}$$

If $\alpha < 0$ the system is in the low barrier regime and the SAR decreases with T. This is illustrated in Fig. 1(b) in dashed lines, where $\alpha = -1/2$. The final temperature, $\Gamma(t\to\infty) = S_0/(a-\alpha)$ is thus smaller than for constant $S(\Gamma) = S_0$. Conversely, in the high barrier regime ($\alpha > 0$), the larger the value of α the more will the system heat. If, albeit positive, $\alpha < a$, the curve will remain concave, as in the dotted curve of Fig. 1(b) where $\alpha = 1/2$. On the other hand, if $\alpha > a$, the heating curve becomes convex, as in the dot-dashed curve in Fig. 1(b) where $\alpha = 3/2$. The condition $\alpha = a$ yields $\Gamma(t) = S_0 t$, as is obviously seen directly from the DE (3).

From Fig. 2(b) it is clear that, even though the SAR may initially increase, it must eventually tend to zero; thus, any heating curve that is initially convex must also eventually present an inflection point. Based on the DE (3) it is straightforward to obtain a general condition for the existence of this point since, on noting that $\dot\Gamma \neq 0$, it suffices that $\ddot\Gamma = 0$. Since $\ddot\Gamma = -a\dot\Gamma + \dot S(\Gamma) = \dot\Gamma[-a + S'(\Gamma)]$, we see that an inflection point will occur if

$$\frac{dS}{d\Gamma} = a. \tag{11}$$

Recalling that $a > 0$, this implies that $S(\Gamma)$ must have a positive slope (over some interval of Γ) — that is, *only systems in the high barrier regime* ($\sigma_0 > \sigma_{m2}$) *may present an inflection point*. Notwithstanding, even in this case, the condition imposed by Eq. (11) may not be met; that is, albeit positive, $S'(\Gamma)$ may never reach the required value a. If we rewrite Eq. (11) as $s'(\Gamma) = a/\xi$, we see that as H_0 increases the right hand side tends quadratically to zero (since $\xi \propto H_0^2$), thence facilitating the appearance of an inflection point. This leads to the important conclusion that quantitative (even substantial) changes in the heating curve that may occur as H_0 increases are not necessarily related to the departure from the linear regime.

In Fig. 3, we present simulated heating curves using Eqs. (3) and (8), for different values of σ_0, fixing $a=1$ and $\omega\tau_0 = 10^{-4}$. In Fig. 3(a) and (b), $\xi = 1$ whereas in Fig. 3(c) and (d), $\xi = 20$. As can be seen, in the first case, the condition (11) is not met for any value of σ_0, even when $s'(\Gamma) > 0$. The relative heating power shown in Fig. 3(a) may thus be directly compared with the initial values of $s(\Gamma\to 0)$ shown in Fig. 2. This, as is commonly discussed in the literature, impinges the idea that in order to optimize the SAR, one must produce samples whose value of σ are as close to σ_{m2} as possible.

On the other hand, note that the entirety of the previous discussion changes when $\xi = 20$, as in Fig. 3(c) and (d). First and foremost, recall that $\xi \propto H_0^2$ so that this 20-fold increase corresponds only to a $\sim$4-fold increase in H_0, which is well within experimental reach. In this condition, the curve for $\sigma_0 = 12$ heats more than that of $\sigma_0 = 10$, and also presents an inflection point, as seen in Fig. 3(d). The curve for $\sigma_0 = 14$ is quite exotic, presenting an inflection point at much larger times. As seen in Fig. 2, this follows because in this case $s(\Gamma)$ is quite small when $\Gamma \sim 0$ (i.e., when $T \sim T_0$). Clearly, results such as this are not in agreement with experimental curves usually reported in the literature, even for high anisotropy samples. The reason for this discrepancy, as is discussed next, is the presence of a size distribution in real samples, which flattens $s(\Gamma)$ considerably.

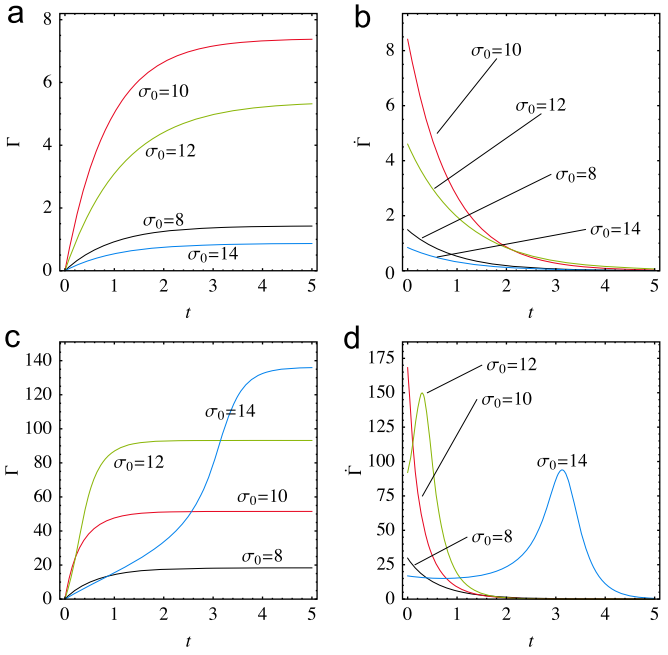

Fig. 3. Simulated heating curves for (a) $\Gamma(t)$ and (b) $\dot\Gamma(t)$, computed using Eqs. (3) and (8), for different values of σ_0, with $a=1$, $\omega\tau_0 = 10^{-4}$ and $\xi = 1$. (c) and (d): similar, but with $\xi = 20$.

5. Poli-disperse systems

For definiteness, we consider a system composed of spherical particles with diameter D distributed according to a lognormal distribution.

We use the notation $x \approx \mathcal{L}(x_0,\delta_x)$ to denote that the random variable x is distributed according to a lognormal distribution with location parameter x_0 and dispersion parameter δ_x according to the probability density function (PDF)

$$p(x;x_0,\delta_x) = \frac{1}{\sqrt{2\pi}x\delta_x}\exp\left[-\frac{\log^2(x/x_0)}{2\delta_x^2}\right]. \tag{12}$$

Analogously to the normal distribution, where sums of normally distributed random variables are also normally distributed, the lognormal distribution satisfy the property that products of lognormally distributed random variables are also lognormally distributed; formally, if $x \approx \mathcal{L}(x_0,\delta_x)$ and $y = ax^n$, then

$$y \approx \mathcal{L}(ax_0^n, n\delta_n) \tag{13}$$

[Note the n-fold increase in the dispersion parameter.] This relation is easily proven starting from the formula $p(y)\,dy = p(x)\,dx$.

Let us now take $D \approx \mathcal{L}(D_0,\delta_D)$. Then, according to the definition $\sigma = Kv/kT$, we have

$$\sigma \approx \mathcal{L}(\sigma_0,\delta_\sigma) = \mathcal{L}\left(\frac{K}{kT}\frac{\pi D_0^3}{6}, 3\delta_D\right). \tag{14}$$

This result has two remarkable consequences, both of which spring from the fact that the fundamental quantity determining the magnetic properties of the particles is the volume, not the diameter. Eq. (14) first shows that there is a 3-fold increase in the dispersion of σ, so that even samples with narrow diameter distributions may suffer a substantial broadening in its volume distribution. Secondly, Eq. (14) implies a substantial enhancement

in the skewness of the distribution. Perhaps the simplest way to visualize this is by examining the ratio between the mean ($D_0 e^{\delta_D^2/2}$) and the median (D_0); i.e., $e^{\delta_D^2/2}$. In the volume distribution, due to the 3-fold increase in the dispersion, this jumps to $e^{9\delta_D^2/2}$; a clearly remarkable enhancement.

Previously, σ_0 denoted the value of σ corresponding to $T=300$, whereas it now represents the location parameter for the PDF (12) in the same condition. This is convenient since both definitions agree when $\delta_\sigma \to 0$. Moreover, as before, the value of σ_0 will change with temperature during the heating curve. This means that the probability density in the variable σ will itself be a function of temperature; viz.,

$$\sigma \approx \mathcal{L}\left(\frac{\sigma_0}{1+\Gamma/T_0}, \delta_\sigma\right).$$

Thus, if we consider the linear response formulas of Section 3, then for each value of Γ the power loss of the ensemble will be an average of Eq. (8) over the PDF (12):

$$\overline{S(\Gamma)} = \xi \int_0^\infty s(\sigma) p\left(\sigma; \frac{\sigma_0}{1+\Gamma/T_0}, \delta_\sigma\right) \mathrm{d}\sigma. \tag{15}$$

Example curves are show in Fig. 4 for $\omega\tau_0 = 10^{-4}$. Each image illustrates curves similar to those in Fig. 2(b), here shown in solid lines to represent mono-disperse samples. Circles, squares and triangles correspond to $\delta_\sigma = 0.1$, 0.2 and 0.4 respectively. As can be seen, due to the asymmetrical nature of the lognormal distribution, a variety of responses are possible. In Fig. 4(a), since $\sigma_0 = 8$ is somewhat far from the maxima $\sigma_{m2} \sim 10.5$ [as shown in Fig. 2(a)], it yields a low SAR for the mono-disperse system. However, on increasing the dispersion, it encompasses values of σ closer to σ_{m2} and thus increase the overall dissipation. The very opposite occurs for $\sigma_0 = 10$, as shown in Fig. 4(b). Notwithstanding, note that in this case the poli-disperse SAR falls much less rapidly than its mono-disperse counterpart. As a consequence, there exists a temperature where the former eventually surpasses the latter. This is an illustration of the "inertia" of poli-disperse systems; that

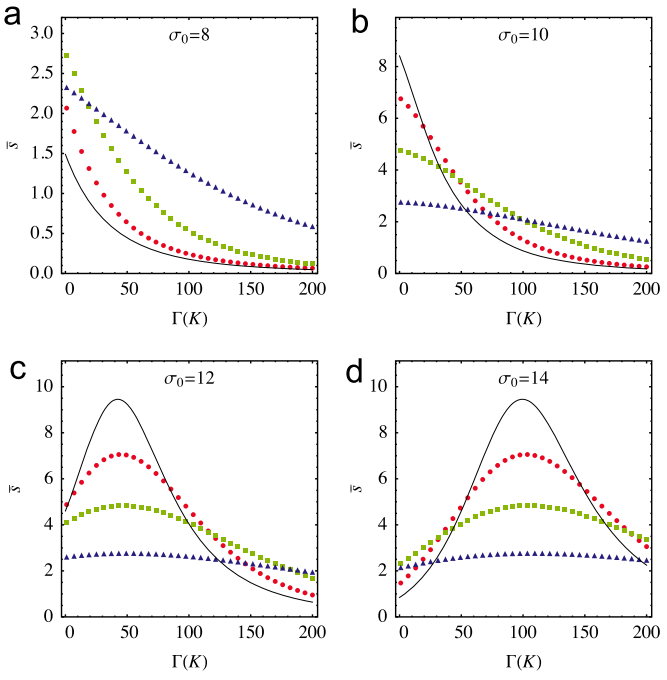

Fig. 4. Temperature dependence of the SAR for poli-disperse samples for $\delta_\sigma = 0.1$ (circles; red), 0.2 (squares; green) and 0.4 (triangles; blue). As usual, $\omega\tau_0 = 10^{-4}$. The mono-disperse SARs, which is the same as those in Fig. 2(b), are shown in solid lines. (For interpretation of the references to color in this figure caption, the reader is referred to the web version of this paper.)

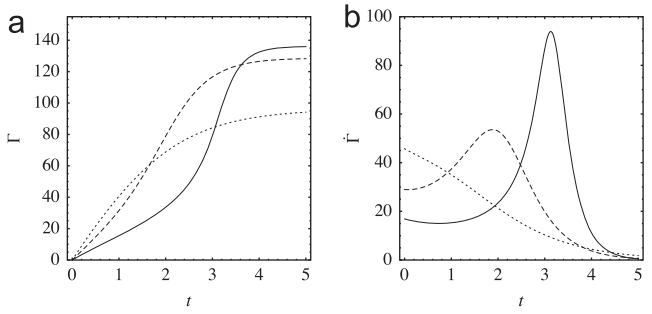

Fig. 5. (a) Heating curves and (b) corresponding time derivative computed from Eq. (3), with the SAR given either by Eq. (8) for a mono-disperse system (solid) or by Eq. (15) for poli-disperse systems, with $\delta_\sigma = 0.1$ (dashed) and $\delta_\sigma = 0.2$ (dotted). Other parameters are $a=1$, $\xi = 20$, $\sigma_0 = 14$ and $\omega\tau_0 = 10^{-4}$ [see also the blue curves in Fig. 3(c) and (d) for $\sigma = 14$]. (For interpretation of the references to color in this figure caption, the reader is referred to the web version of this paper.)

is, a larger δ_σ yields a SAR that tends to remain roughly constant over a broad range of temperatures. This result, contrarily to our previous discussion, partially corroborates the use of the Box–Lucas function [Eq. (5)].

With respect to the high barrier cases, illustrated in Fig. 4(c) and (d) for $\sigma_0 = 12$ and 14 respectively, it now becomes clear that increasing δ_σ substantially reduces the initial positive slope of $S(\Gamma)$, as argued in the end of Section 4. As a further illustration of this effect, Fig. 5 presents a comparison of the heating curves for $\sigma_0 = 14$. The mono-disperse result, which corresponds to the blue curve in Fig. 2(c) and (d), is shown as a solid line; its poli-disperse counterparts, for $\delta_\sigma = 0.1$ and 0.2, are shown in dashed and dotted lines respectively. As can be seen, the inflection point is significantly shifted to smaller times in the former case and disappears completely in the latter. This effect is quite remarkable, in the sense that $\delta_\sigma = 0.1$ means $\delta_D \sim 0.03$ which, for all practical purposes, correspond a mono-disperse system. We thus reach the important conclusion that the 3-fold increase in the dispersion of σ produces marked changes in the heating properties of the material, which can only be accounted for by properly replacing Eq. (8) with Eq. (15).

6. Computing the SAR from experimental data

A cooling curve well described by a single exponential strongly corroborate the use of the present model. If this is indeed the case, then it is possible to devise a simple method to compute the temperature dependence of the SAR from the experimental heating curve, which holds regardless of the underlying dissipation model. The method requires only that a is known (i.e., is fitted from the cooling curve). The steps are:

(i) Compute $\dot{\Gamma}(t)$ from $\Gamma(t)$;
(ii) Construct the function $S(t) = \dot{\Gamma}(t) + a\Gamma(t)$;
(iii) Graph a parametric curve $(\Gamma(t), S(t))$ to yield $S(\Gamma)$.

Step (i) is clearly the most troublesome since differentiating data greatly magnifies even the slightest fluctuations. Several methods exist to remedy this deficiency. Among them we recommend either Smoothing Splines [25] or the Savitzky–Golay filter [26]; both fit local polynomials, thus allowing the derivative to be computed by differentiating the fitted functions analytically. Gaussian and Wiener filter may also be employed to smooth the data and thence compute the derivative by finite differencing.

The procedure is illustrated in Fig. 6. The data, depicted by open circles, was generated considering a poli-disperse system [Eqs. (3) and (15)] with $a=1$, $\xi = 20$, $\sigma_0 = 12$, $\delta_\sigma = 0.1$ and

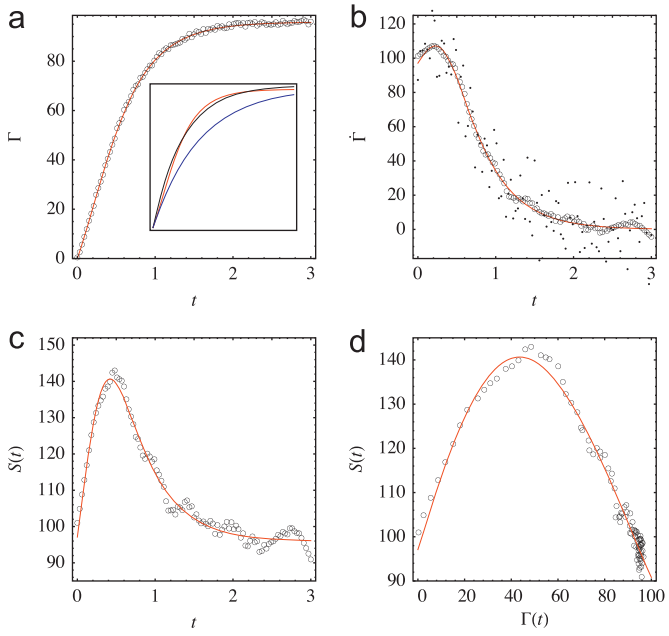

Fig. 6. Procedure to compute the temperature dependence of the SAR from the experimental data. The heating curve was simulated from Eqs. (3), (8) and (15) with $a=1$, $\xi=20$, $\sigma_0=12$, $\delta_\sigma=0.1$ and $\omega\tau_0=10^{-4}$. Red solid lines denote the exact solution and open circles the simulated data, with added random noise. (a) Heating curve, $\Gamma(t)$; (b) $\dot{\Gamma}(t)$ computed using a Savitzky–Golay filter with quadratic polynomials and a 5-point centered window; the scattered points denote $\dot{\Gamma}(t)$ computed from centered finite differencing. (c) $S(t)=\dot{\Gamma}(t)+a\Gamma(t)$. (d) Parametric plot of $(\Gamma(t),S(t))$ yielding $S(\Gamma)$. The inset in image (a) shows a comparison between the exact solution (red), a Box–Lucas fit [Eq. (5)] yielding $a=1.54$ and $S_0=152$ (black), and the same function computed using the exact values $a=1$ and $S_0=S(\Gamma=0)\simeq 97$ (blue). (For interpretation of the references to color in this figure caption, the reader is referred to the web version of this paper.)

$\omega\tau_0=10^{-4}$. To mimic real situations, random noise was also added. In each image, the exact solution is depicted in red for comparison. We note that the SAR for this condition was presented in Fig. 4(c) as red circles.

The heating curve is shown in Fig. 6(a), where it is seen to present a subtle inflection point at small times. This is also visible from the maxima in Fig. 6(b), where $\dot{\Gamma}(t)$ was computed using the Savitzky–Golay filter with quadratic polynomials and a 5-point centered window. The scattered solid points in Fig. 6(b) illustrate the unacceptably high level of noise that results from computing the derivative [26] using simple centered differencing $[f'(x)=(f(x+h)-f(x-h))/(2h)]$. In passing, it is worth noting that this is nonetheless still vastly superior than forward differencing $[f'(x)=(f(x+h)-f(x))/h]$. The step (ii) above is illustrated in Fig. 6(c) where the time dependence of the SAR is computed. Finally, in Fig. 6(d) a parametric plot yields the desired temperature dependence.

The inset in Fig. 6(a) serves to illustrate an important point concerning the Box–Lucas Eq. (5). The red curve is the exact solution (same as in the main figure); the blue curve was computed from Eq. (5) with $a=1$ and $S_0\simeq 97$, which is the value of $S(\Gamma\to 0)$ for the present conditions [cf. Fig. 6(d)]. As one might expect, albeit agreeing at very short times, it yields an entirely different response. The black curve, on the other hand, corresponds to a fit of the data using Eq. (5). The best fit parameters were $a=1.54$ and $S_0=152$. Note how these values are entirely false, even though the agreement between the fit and the exact solution is roughly acceptable. On the one hand, this indicates that great care must be taken in using Eq. (5). On the other, it also emphasizes the fundamental importance of the cooling curve, from which a could have been unambiguously determined.

7. Two-temperatures model

We have thus far assumed that the entire medium has a uniform temperature. However, it is a known experimental fact that the nanoparticles reach temperatures far greater than that of its encompassing fluid. In this section we propose a simple (or perhaps the simplest) model to account for this temperature difference. As before, the large number of particles and their random spatial arrangement suggest an approach based on average quantities. Fig. 7 illustrates the setup: the nanoparticles have an average temperature T_1 and dissipate heat in the fluid whose temperature is T_2. The fluid, in turn, interacts with the heat bath that is maintained at a fixed temperature T_0. The experiment, we note, is only capable of measuring T_2.

A generalization of Eq. (3) then reads

$$\begin{aligned}\dot{\Gamma}_1&=a(\Gamma_2-\Gamma_1)+S(\Gamma_1),\\ \dot{\Gamma}_2&=a(\Gamma_1-\Gamma_2)-2b\Gamma_2,\end{aligned}\tag{16}$$

where a and b are constants (unrelated to the previous ones) and the factor of 2 was inserted for convenience. In this model the particles exchange heat with the fluid via a transfer rate a and the fluid exchanges heat with the thermal bath via $2b$. In matrix notation let $\boldsymbol{\Gamma}=(\Gamma_1,\Gamma_2)$ and $\boldsymbol{S}=(S(\Gamma_1),0)$ be column vectors. Then

$$\dot{\boldsymbol{\Gamma}}=-A\boldsymbol{\Gamma}+\boldsymbol{S},\quad A=\begin{bmatrix}a & -a\\ -a & a+2b\end{bmatrix}.\tag{17}$$

The matrix A is both symmetric and positive definite and thence has both eigenvalues real and positive, as expected. They are $\lambda_1=a+b+\sqrt{a^2+b^2}$ and $\lambda_2=a+b-\sqrt{a^2+b^2}$. Since $\boldsymbol{\Gamma}(t=0)=(0,0)$, the general solution is simply

$$\boldsymbol{\Gamma}(t)=\int_0^t e^{-A(t-t')}\,\boldsymbol{S}\,dt'=(I-e^{-At})A^{-1}\boldsymbol{S},\tag{18}$$

where I is the identity matrix and e^{-At} is the matrix exponential solution for $-A$.

Let us focus on the solution for a constant heat source $S(\Gamma_1)=S_0$, which can be easily shown to be

$$\begin{aligned}\Gamma_1(t)&=\frac{S_0}{2\sqrt{a^2+b^2}}[(\lambda_1-a)f_2(t)-(\lambda_2-a)f_1(t)],\\ \Gamma_2(t)&=\frac{S_0 a}{2\sqrt{a^2+b^2}}[f_2(t)-f_1(t)],\end{aligned}\tag{19}$$

where $f_i(t)=(1-e^{-\lambda_i t})/\lambda_i$ is a "Box–Lucas factor". It is worth noting that this function has the property that, because $\lambda_1>\lambda_2$, $f_1(t)<f_2(t)$ for all t.

The key point to note concerning the solution in Eq. (19) is that, in general, $a\ll b$, since these constants depend on the characteristic length of each element. It then follows that $\lambda_1\gg\lambda_2$ and $f_1(t)\ll f_2(t)$. In this limit it can be shown from

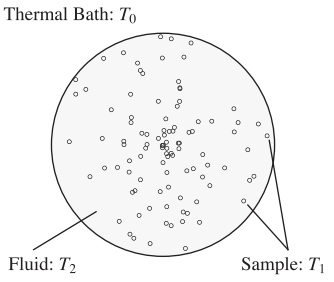

Fig. 7. Schematic description of the two-temperatures model: the particles are represented by a single temperature T_1 and dissipate heat to the fluid whose temperature is T_2. The latter, in turn, interacts with the thermal bath maintained at a fixed temperature T_0. We assume that the experiment measures T_2.

Eq. (19) that

$$\frac{\Gamma_1}{\Gamma_2} \simeq \frac{2b}{a}. \tag{20}$$

It is thus seen that throughout the heating process, the temperature of the particles is always larger than that of the fluid by a factor of $2b/a \gg 1$. Intuitively, this factor is the ratio between the rate at which the fluid dissipates heat to the environment and the rate at which the particles dissipate heat to the fluid. This result shows that this simple model is indeed capable of capturing the key aspect we sought. Unfortunately, to actually infer the temperature of the particles would require knowledge of a and b, the former not being readily available through experiment.

As a final comment, the two-temperatures model predicts, for both the heating and cooling curves, response-time phenomena similar to that discussed in the previous sections. As mentioned, those are related either to a response time of the experimental setup or to the thermal radiation stemming from the coils. However, it is our belief that since $a \ll b$, the present contribution should be negligible compared to the others.

8. Discussion and conclusions

In this paper we discussed in detail a simple theoretical model capable of describing the heating curve in magnetic hyperthermia experiments. Its simplicity is simultaneously its greatest advantage and limitation; advantage in the sense that specific properties of a given experimental setup are described by simple parameters appearing in the model, which can thus be fitted from experiment; and limitation in the sense that it cannot be extended beyond the lumped-element approximation (i.e., it may not serve as a starting point for more elaborate models involving, for instance, the heat equation). Another merit of the present approach is the ability to connect the calorimetric and magnetic properties of the system with great simplicity. Since the power loss enters merely as a forcing term in the heating differential equation, it is quite trivial to test and investigate different models for it. An example, not pursued in the present paper, is the linear response theory for Brownian relaxation instead. Another would be, for instance, the non-linear response for Néel relaxation. In this case, the magnetic response must be computed numerically for each temperature and condition of the external field. Notwithstanding, an interpolating function for $S(\Gamma)$ may still be easily constructed from simulations at different temperatures.

The present discussion also served to illustrate the importance of the cooling curve. In fact, because this curve is entirely non-magnetic, it enables one to extract all thermal properties of the sample. This, in turn, leaves only magnetic parameters to be studied in the heating curve, greatly facilitating the analysis. As an example, consider the influence of the heat stemming from the coils which generate the magnetic field. Midway through the heating curve this may start to become significant, presenting itself as a different slope in the heating curve. However, the heating and cooling properties of the coil are described by the same time constant and should thence appear at the initial instants of the cooling curve [cf. Fig. 1(a)]. With such knowledge, one may safely discern if changes in the heating curve spring from the nanoparticles or the apparatus.

We have also shown that depending on the properties of the magnetic sample, it may be important to take into account the temperature variation of the SAR during the measurement of the heating curve. In particular, if the particles are initially blocked at ambient temperature (with respect to the frequency in question), then the SAR as a function of temperature will initially present a positive slope. However, since it must eventually tend to zero as T becomes sufficiently high, the heating curve may present an inflection point. We have also shown that, within the scope of the linear response theory, increasing the magnetic field facilitates the appearance of this inflection point. This means that changes in the shape of the heating curve are not necessarily related to a departure from the linear regime, a quite relevant conclusion.

Significant information can be obtained by sequential measurements of the SAR for different field amplitudes. The reason, at least within the scope of the linear response, is that the only quantity changing in Eq. (15) is $\xi \propto H_0^2$. Thus, combining knowledge from the size distribution from a morphological analysis may possibly yield important parameters, such as σ_0 or τ_0.

Finally, we would like to note the following possibility which, to our knowledge, has never been pursued in an experiment. Irrespective of the models discussed in this paper, the SAR at ambient temperature may always be computed from the usual formula, Eq. (4). However, it is also possible to repeat the experiment at different starting temperatures (i.e., different "ambient" temperatures). In this form one may construct the function $S(T)$ without the need for any underlying models. While measuring the SAR at different temperatures may be of no interest to biological applications, it may yield important information regarding the energy barrier distribution of the system.

Acknowledgments

The author acknowledges Prof. Andris F. Bakuzis for stimulating discussions. This work was funded by the Brazilian funding agency FAPESP.

References

[1] J.-H. Lee, J.-T. Jang, J.-s. Choi, S.H. Moon, S.-h. Noh, J.-w. Kim, J.-G. Kim, I.-S. Kim, K.I. Park, J. Cheon, Exchange-coupled magnetic nanoparticles for efficient heat induction, Nature Nanotechnology 6 (January) (2011) 418–422.
[2] R. Hergt, W. Andra, C. D'Ambly, Physical limits of hyperthermia using magnetite fine particles, IEEE Transactions on Magnetics 34 (5) (1998) 3745–3754.
[3] J. Carrey, B. Mehdaoui, M. Respaud, Simple models for dynamic hysteresis loop calculations of magnetic single-domain nanoparticles: application to magnetic hyperthermia optimization, Journal of Applied Physics 109 (8) (2011) 083921.
[4] Q.A. Pankhurst, N.K.T. Thanh, S.K. Jones, J. Dobson, Progress in applications of magnetic nanoparticles in biomedicine, Journal of Physics D: Applied Physics 42 (November) (2009) 224001.
[5] J. Dobson, Magnetic nanoparticles for drug delivery, Nano Today 2 (3) (2006) 22–32.
[6] I. Sharifi, H. Shokrollahi, S. Amiri, Ferrite-based ferrofluids used in hyperthermia applications, Journal of Magnetism and Magnetic Materials 324 (October) (2012) 903–915.
[7] M. Kishimoto, M. Minagawa, H. Yanagihara, T. Oda, N. Ohkochi, E. Kita, Synthesis and magnetic properties of platelet γ-Fe_2O_3 particles for medical applications using hysteresis-loss heating, Journal of Magnetism and 'Magnetic Materials 324 (April) (2012) 1285–1289.
[8] R. Hergt, R. Hiergeist, I. Hilger, W. Kaiser, Y. Lapatnikov, S. Margel, U. Richter, Maghemite nanoparticles with very high AC-losses for application in RF-magnetic hyperthermia, Journal of Magnetism and Magnetic Materials 270 (April) (2004) 345–357.
[9] C. Bean, I. Jacobs, Magnetic granulometry and super-paramagnetism, Journal of Applied Physics 27 (12) (1956) 1448–1452.
[10] L. Néel, Théorie du traînage magnétique des ferromagnétiques en grain fins avec application aux terres cuites, Annales de Geophysique 5 (1949) 99.
[11] W.F. Brown, Thermal fluctuations of single-domain particles, Physical Review 130 (5) (1963) 1677–1686.
[12] W.T. Coffey, Y.P. Kalmykov, J.T. Waldron, The Langevin Equation. With Applications to Stochastic Problems in Physics, Chemistry and Electrical Engineering, 2nd ed., World Scientific Publishing Co, Pvt. Ltd., Singapore, 2004.
[13] J.L. Dormann, F. Lucari, F. D'Orazio, E. Tronc, P. Prené, J.P. Jolivet, D. Fiorani, R. Cherkaoui, M. Noguès, Thermal variation of the relaxation time of the magnetic moment of Fe_2O_3 nanoparticles with interparticle interactions of various strengths, Physical Review B 53 (21) (1996) 291–297.

[14] P. Gambardella, S. Rusponi, M. Veronese, S.S. Dhesi, C. Grazioli, a. Dallmeyer, I. Cabria, R. Zeller, P.H. Dederichs, K. Kern, C. Carbone, H. Brune, Giant magnetic anisotropy of single cobalt atoms and nanoparticles, Science (New York, N.Y.) 300 (May) (2003) 1130–1133.
[15] K.M. Krishnan, Advances in magnetics biomedical nanomagnetics: a spin through possibilities in imaging, diagnostics, and therapy, IEEE Transactions on Magnetics 46 (7) (2010) 2523–2558.
[16] R.K. Gilchrist, R. Medal, W.D. Shorey, R.C. Hanselman, J.C. Parrott, C.B. Taylor, Selective inductive heating of lymph nodes, Annals of Surgery 146 (October) (1957) 596–606.
[17] D.-H. Kim, E.A. Rozhkova, I.V. Ulasov, S.D. Bader, T. Rajh, M.S. Lesniak, V. Novosad, Biofunctionalized magnetic-vortex microdiscs for targeted cancer-cell destruction, Nature Materials 9 (March) (2010) 165–171.
[18] I. Hilger, R. Hergt, Use of magnetic nanoparticle heating in the treatment of breast cancer, Nanobiotechnology, IEE 152 (2005) 33–39.
[19] E.L. Verde, G.T. Landi, J.A. Gomes, M.H. Sousa, A.F. Bakuzis, Magnetic hyperthermia investigation of cobalt ferrite nanoparticles: comparison between experiment, linear response theory and dynamic hysteresis simulations, Journal of Applied Physics 111 (2012) 123902.
[20] D.E. Bordelon, C. Cornejo, C. Gruttner, F. Westphal, T.L. DeWeese, R. Ivkov, Magnetic nanoparticle heating efficiency reveals magneto-structural differences when characterized with wide ranging and high amplitude alternating magnetic fields, Journal of Applied Physics 109 (12) (2011) 124904.
[21] G. Bertotti, Hysteresis in Magnetism, 1st ed., Academic Press, 1998.
[22] R. Kubo, Statistical–mechanical theory of irreversible processes. 1. General theory and simple applications to magnetic and conduction problems, Journal of the Physical Society of Japan 12 (6) (1957) 570.
[23] M. Shliomis, V.I. Stepanov, Frequency dependence and long time relaxation of the susceptibility of the magnetic fluids, Journal of Magnetism and Magnetic Materials 122 (April) (1993) 176–181.
[24] M. Abramowitz, I. Stegun, Handbook of Mathematical Functions, Dover, New York, 1964.
[25] K. Ahnert, M. Abel, Numerical differentiation of experimental data: local versus global methods, Computer Physics Communications 177 (November) (2007) 764–774.
[26] W.H. Press, S.A. Teukolsky, W.T. Vetterling, B.P. Flannery, Numerical Recipes, 3rd ed., Cambridge University Press, New York, 2007.